3. (a) A. Kuramata, S. Yamazaki, and K. Nakajima, Extended Abstracts of "22nd Conf. on Solid State Devices and Materials," Jpn. Soc. Appl. Phys., Aug. 22, 1990; (b) R. R. Saxena, J. E. Fouquet, V. M. Sardi, and R. L. Moon, *Appl. Phys. Lett.*, **53**, 304 (1988).
4. P. Daniel, H. D. Sarge, and W. Weiner, "Proc. VII Intl. Conf. on Ion Implantation Technology," July 30, 1990, Surrey, England.
5. (a) D. Kotecki, J. Blouse, C. Parks, and S. Sarkozy, "Proc. MRS Symposium on Chemical Perspectives in Microelectronics," Nov. 26, 1990, Boston, MA; (b) T. E. Tang, in "Technical Digest International Electron Device Conference," IEEE, New York (1989).
6. (a) D. S. Williams and E. A. Dein, *This Journal*, **134**, 657 (1987); (b) W. Kern and R. C. Heim, *ibid.*, **117**, 562 (1970).
7. C. L. Keller and P. L. Tucker, "Hazardous Materials Regulations of the Department of Transportation," U.S. Bureau of Explosives, Washington, DC (1987).
8. N. M. Gralenski, *Microelectron., Manufact. Test.*, **10**, 2 (1987).
9. W. Kern, W. A. Kurylo, and C. J. Tino, *RCA Rev.*, **46**, 117 (1985).
10. M. Shibata, T. Yoshimi, and K. Sugawara, *This Journal*, **122**, 157 (1975).
11. S. M. Sze, "VLSI Technology," McGraw-Hill, Inc., New York (1983).
12. W. Kern, G. L. Schnable, and A. W. Fischer, *RCA Rev.*, **37**, 3 (1976).

Modeling and Optimization of the Step Coverage of Tungsten LPCVD in Trenches and Contact Holes

A. Hasper, J. Holleman, and J. Middelhoek[1]

Faculty of Electrical Engineering, University of Twente, 7500 AE Enschede, The Netherlands

C. R. Kleijn and C. J. Hoogendoorn

Faculty of Applied Physics, Delft University of Technology, 2600 GA Delft, The Netherlands

ABSTRACT

A model is presented to calculate the step coverage of blanket tungsten low pressure chemical vapor deposition (W-LPCVD) from tungsten hexafluoride (WF_6). The model can calculate tungsten growth in trenches and circular contact holes, in the case of the WF_6 reduction by H_2, SiH_4, or both. The step coverage model predictions have been verified experimentally by scanning electron microscopy (SEM). We found that the predictions of the step coverage model for the H_2 reduction of WF_6 are very accurate, if the partial pressures of the reactants at the inlet of the trench or contact hole are known. To get these reactant inlet partial pressures, we used a reactor model which calculates the surface partial pressures of all the reactants. These calculated surface partial pressures are used as input for our step coverage model. In this study we showed that thermodiffusion plays a very important role in the actual surface partial pressure. In the case where SiH_4 was present in the gas mixture trends are predicted very well but the absolute values predicted by the step coverage model are too high. The partial pressure of HF, which is a by-product of the H_2 reduction reaction, may be very high inside trenches or contact holes, especially just before closing of the trench or contact hole. We found no influence of the calculated HF partial pressure on the step coverage. Differences between step coverage in trenches and contact holes, as predicted by the step coverage model, were found to agree with the experiments. It is shown that the combination of the step coverage and reactor model is very useful in the optimization towards high step coverage, high throughput, and low WF_6 flow. We found a perfect step coverage (no void formation) in a 2 μm wide and 10 μm deep (2 × 10 μm) trench using an average WF_6 flow of only 35 sccm, at a growth rate of 150 nm/min. In general, it is shown that the reduction of WF_6 by SiH_4 offers no advantages over the reduction by H_2 as far as step coverage is concerned.

With the increasing degree of complexity in integrated circuits the aspect ratio of contacts and vias also increases. These geometries require deposition techniques capable of filling submicron high aspect ratio contact holes without void formation. Blanket tungsten, deposited by LPCVD and subsequent back etching (Fig. 1a), is widely used to fill these contacts (1, 2). A second possibility is to fill these contacts using a selective deposition scheme (3-11), in order to avoid the need of back etching (see Fig. 1b). An advantage of selective over blanket deposition of tungsten is the economic use of WF_6. However, selective deposition of tungsten is only possible when all the contacts are equal in depth (12), which is not always the case (see Fig. 2). Other disadvantages of selective deposition of tungsten are the sensitivity to pretreatments and the nonreproducibility.

To deposit tungsten two reducing agents are widely used. First the H_2 reduction reaction of WF_6 with the following overall reaction

$$WF_6 + 3H_2 \rightarrow W + 6HF \quad [1]$$

Second, the SiH_4 reduction reaction of WF_6

$$2WF_6 + 3SiH_4 \rightarrow 2W + 3SiF_4 + 6H_2 \quad [2]$$

The H_2 reduction reaction has shown its excellent step coverage (1, 2), but it has some disadvantages compared to the SiH_4 reduction reaction such as low and very temperature dependent growth rate (3-5) and rough layers (1, 2, 13). The SiH_4 reduction reaction however has a high and nearly temperature independent growth rate and results in layers with a small grain size (1, 11, 13, 14). The reactivity of WF_6 with silicon in the case of the SiH_4 reduction reaction is much less than the H_2 reduction reaction. The WF_6 reaction with silicon results in the undersirable gouging and encroachment of silicon.

The problem of step coverage has been evaluated in the case of physical vapor deposition (PVD) (24). In that case,

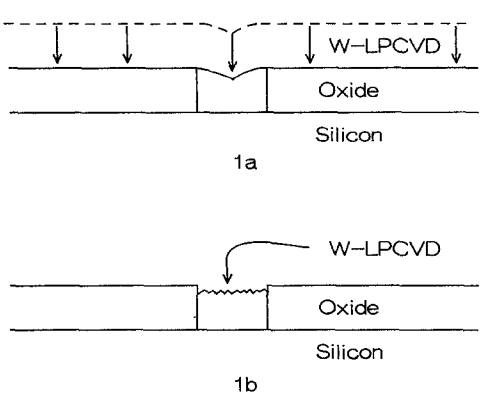

Fig. 1. (a) Blanket deposition of tungsten and subsequent back-etching and (b) selective deposition of tungsten.

[1] Deceased.

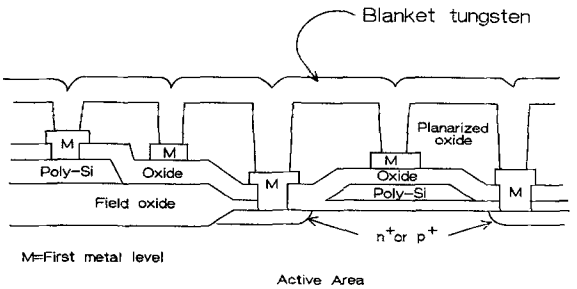

Fig. 2. Differences in contact depths that may be present after planarization.

the step coverage is dominated by geometrical sidewall shadowing and surface diffusion. This approach is not applicable for CVD processes. McConica *et al.* (15) were the first to propose that W-LPCVD in circular contact holes could be described by the simultaneous heterogeneous reaction on the side wall and diffusion along the contact hole. Our step coverage model is also based on these assumptions. In this report we extend the model of McConica *et al.* to a numerical W-LPCVD model for zero- and first-order reactions allowing other geometries (like trenches) and accounting for tungsten growth on the bottom of the geometry in the model boundary conditions.

The step coverage of W-LPCVD has been investigated experimentally as well as theoretically (1, 2, 15-23). However, using the combination of the output of a reactor model as input for a step coverage model for the reduction of WF_6 by H_2 and/or SiH_4 has not been reported yet. For the H_2 reduction reaction an analytical solution of the step coverage can be found in terms of deposition parameters ignoring tungsten growth at the bottom of the features (15). For the SiH_4 reduction reaction no such analytical solution can be obtained and numerical methods are necessary.

Theory

In our study we defined the step coverage as the ratio in percents of the tungsten thickness (a) taken halfway the feature depth and the substrate surface thickness (b) at the moment the feature closes. This definition is shown in Fig. 3. Thus we obtain 100% step coverage if no void formation occurs.

Knudsen diffusion.—At the pressures (100 Pa) and temperatures (673 K) common in W-LPCVD, the mean-free path for the reactants is about 100 μm. This is much larger than the typical feature diameter. Whenever the mean-free path of the reactants is larger than the diameter of the feature (25, 26), Knudsen diffusion is the dominating mechanism for mass transfer. Because the Knudsen diffusion rate is much smaller than bulk diffusion, concentration gradients can occur easily during the growth. The reactants move into the feature by random flights interrupted by collisions and momentary adsorption on the wall. The gas flow is delayed by the wall resistance. This is the so-called Knudsen flow. According to the kinetic theory of gases (25, 26), the Knudsen diffusion coefficient can be written as follows.

For a contact hole with radius r

$$D_{k,\infty} = \frac{2}{3} \cdot r \cdot \left(\frac{8\,RT}{\pi M}\right)^{1/2} \quad [3a]$$

And for a trench with a width w

$$D_{k,\infty} = \frac{2}{3} \cdot w \cdot \left(\frac{8RT}{\pi M}\right)^{1/2} \quad [3b]$$

From Eq. [3a] and [3b] the diffusivities of the reactants in infinitely long circular or rectangular tubes are known, however, in practice the aspect ratio is not infinite and the influence of the open end of the feature has to be considered. We have a molecular flow through an open end and a short tube. The tube conductance has to be corrected with a factor depending on the finite length and the influence of the diameter of the feature. This is investigated by Clausing (27), who found a rather complicated expression for this phenomenon. Dushman (26) derived an expression which is an approximation of the so-called Clausing's factor (K'). This approximation is accurate within 10% compared to the Clausing's factor. The Knudsen diffusion coefficient corrected with this factor for circular contact holes is

$$D_k = D_{k,\infty} \cdot K' = \frac{2}{3} \cdot r \cdot \left(\frac{8RT}{\pi M}\right)^{1/2} \cdot \left(\frac{1}{1 + 8 \cdot r/3 \cdot 1}\right) \quad [4a]$$

For trenches

$$D_k = D_{k,\infty} \cdot K' = \frac{2}{3} \cdot w \cdot \left(\frac{8RT}{\pi M}\right)^{1/2} \cdot \left(\frac{1}{1 + 8 \cdot w/3 \cdot 1}\right) \quad [4b]$$

During the growth, the dimensions of the feature are changing, thus making these diffusion coefficients become time dependent. For the calculation of the step coverage we will use the following two equations.

For contact holes

$$D_k\,[r(t), l(t)] = \frac{2}{3} \cdot r(t) \cdot \left(\frac{8RT}{\pi M}\right)^{1/2} \cdot \left(\frac{1}{1 + 8 \cdot r(t)/3 \cdot l(t)}\right) \quad [5a]$$

For trenches

$$D_k\,[w(t), l(t)] = \frac{2}{3} \cdot w(t) \cdot \left(\frac{8RT}{\pi M}\right)^{1/2} \cdot \left(\frac{1}{1 + 8 \cdot w(t)/3 \cdot l(t)}\right) \quad [5b]$$

Some remarks have to be made concerning these diffusion coefficients. First, these formulas are derived for tubes without bottoms. In reality molecules can bounce back, but for high aspect ratio features, as studied in this paper, the influence of the bottom will be small. Second, the formulas are derived for features, which are regarded as being constant in cross section across the length. For high aspect ratio trenches and contact holes this is approximately the case during growth.

The hydrogen reduction reaction.—During typical W-LPCVD conditions, the tungsten deposition rate from H_2 and WF_6, appears to be fully determined by surface chemistry. The overall reaction is given by reaction [1] and the growth rate is given by

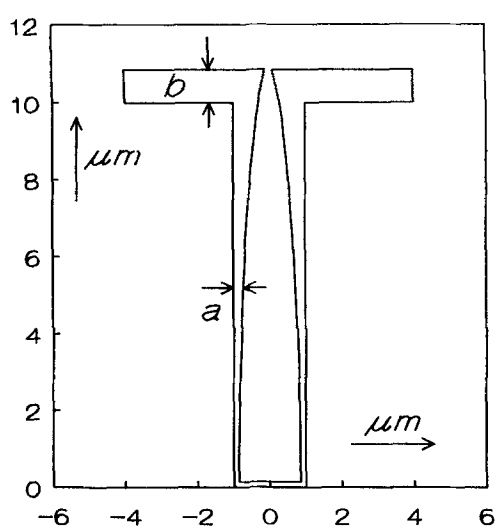

Fig. 3. Schematic sketch of a cross section of a trench or a contact hole. Our definition of the step coverage (S.C.) S. C. = a/b * 100%.

$$R_H = c_1 \cdot [p(WF_6)]^0 \cdot [p(H_2)]^{1/2} \cdot \exp(-E_A/RT) \quad \text{for } p(WF_6) > 0 \quad [6a]$$

$$R_H = 0 \quad \text{for } p(WF_6) = 0 \quad [6b]$$

Recently, it was found that the deposition rate is indeed zero-order down to very low pressures of WF_6 (28, 38). In the literature (3-5, 28-30) E_A is found to be 67-73 kJ/mol. Based on the extensive experimental set published by Broadbent and Ramiller (3), E_A is taken at 69 kJ/mol and $c_1 = 1.7 \times 10^{-4}$ mol · $Pa^{-1/2}$ · cm^{-2} · s^{-1}. These values were shown to be in good agreement with our own experiments. Because E_A and c_1 were derived from experiments in a hot wall system, the values are not suffering from uncertainties in the wafer temperature.

The silane reduction reaction.—WF_6 can also be reduced by SiH_4 (6-10) and other higher order silanes (8). The reaction with SiH_4 takes place according to reaction [2] (31). In the literature only a few publications deal with the SiH_4 reduction reaction of WF_6. References (11, 14) as well as our own observations (see Fig. 4) indicate that the growth rate is first order in the partial pressure of SiH_4, and nearly independent of the temperature in the examined region of 523 to 673 K. The deposition rate is also zero order in WF_6. The deposition rate of the SiH_4 reduction reaction can be written as

$$R_s = c_2 \cdot [p(WF_6)]^0 \cdot [p(SiH_4)]^1 \quad \text{for } p(WF_6) > 0 \quad [7a]$$

$$R_s = 0 \quad \text{for } p(WF_6) = 0 \quad [7b]$$

In Eq. [7] $C_2 = 1.0 \times 10^{-8}$ mol · cm^{-2} · s^{-1} · Pa^{-1}. In our modeling study Eq. [6] and [7] are used to calculate the growth rate.

Mathematical model of deposition in trenches and contact holes.—The model is based on a one-dimensional mass balance in a contact hole or trench. For this model the following assumptions have to be made; (*i*) the reaction only takes place on the wall and bottom, (*ii*) there is no surface diffusion, (*iii*) the lateral concentration gradients are negligible. With these assumptions the concentration profile in the trench or contact hole can be calculated. Consider a schematic diagram of a volume element V of a trench as represented in Fig. 5

$$\frac{\partial(C_i \cdot V)}{\partial t} = (\text{Flux}_{in} \cdot A)\Big|_{x=x_1} - (\text{Flux}_{out} \cdot A)\Big|_{x=x_2} - R(C_i, T) \cdot \eta \cdot A_A \quad [8]$$

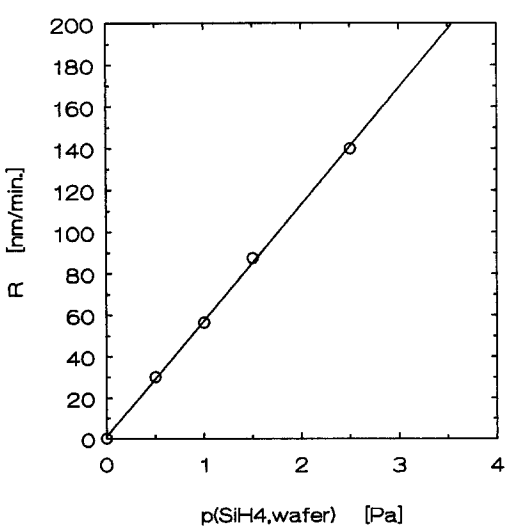

Fig. 4. Growth rate as a function of the partial pressure of SiH_4 (T_{wafer} = 673 K, P_{tot} = 133 Pa, Ar = 1.5 slm, and WF_6 = 150 sccm).

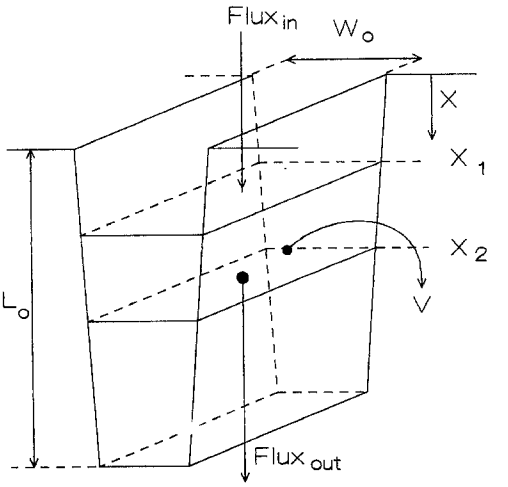

Fig. 5. A schematic drawing of a differential element in a trench.

Here $R(C_i, T)$ is the molar rate of WF_6 disappearance per unit surface area as a function of the local molar concentration C_i and the absolute temperature T, η is a stoichiometry constant depending on the chemistry. A_A is the active surface of the volume element V over which the reaction takes place. A is the cross-sectional area of the trench or contact hole. In our step coverage study we considered two geometries

I. A rectangular trench with initial width W_0 and initial depth L_0.

II. A circular contact hole with initial radius R_0 and initial depth L_0.

For these two geometries this results in the following differential equations for the molar concentrations C_i as given by the following.

For trenches

$$\frac{\partial(C_i \cdot w)}{\partial t} = \frac{\partial}{\partial x}\left\{w \cdot D_k \cdot \frac{\partial C_i}{\partial x}\right\} - 2 \cdot R(C_i, T) \cdot \eta \quad [9a]$$

For contact holes

$$\frac{\partial(C_i \cdot r^2)}{\partial t} = \frac{\partial}{\partial x}\left\{r^2 \cdot D_k \cdot \frac{\partial C_i}{\partial x}\right\} - 2 \cdot R(C_i, T) \cdot \eta \cdot r \quad [9b]$$

Where the variables C_i, w, r, and D_k are functions of the position and time. Now from Eq. [9a] and [9b] and according to reaction [1] or/and [2] we can write a set of differential equations for the WF_6, SiH_4, H_2, SiF_4, and HF concentration. For example the differential equation of the WF_6 concentration in a trench becomes

$$\frac{\partial\{C_w \cdot w(x, t)\}}{\partial t} = \frac{\partial}{\partial x}\left\{w(x, t) \cdot D_k^w \cdot \frac{\partial C_w}{\partial x}\right\} - 2 \cdot \{R_H(C_H, C_W, T) + R_S(C_S, C_W)\} \quad [10]$$

The changing diameters of the features are given by the following differential equations

For trenches

$$\frac{\partial w(x, t)}{\partial t} = -2 \cdot \frac{\{R_S(C_W, C_S) + R_H(C_W, C_H, T)\}}{\rho_W} \quad [11a]$$

For contact holes

$$\frac{\partial r(x, t)}{\partial t} = -\frac{\{R_S(C_W, C_S) + R_H(C_W, C_H, T)\}}{\rho_W} \quad [11b]$$

By solving the partial differential equations for all reactants, the concentration of WF_6, SiH_4, H_2, SiF_4, and HF can be determined. From these concentrations the growth rate

at any point in the trench or in the contact hole can be calculated and thus the deposition profile and the step coverage (see Fig. 3).

Suppose that the reactor is operating under steady-state conditions, the concentrations of the reactants at the mouth of the feature are constant. The initial conditions for the partial differential equations, for all x, are

$$C_i(x, 0) = C_{i,0} \quad [12a]$$

$$r(x, 0) = R_0 \quad \text{(contact holes)} \quad [12b]$$

$$w(x, 0) = W_0 \quad \text{(trenches)} \quad [12c]$$

$$l(0) = L_0 \quad [12d]$$

The boundary conditions for the concentration C_i, for all t, are

$$x = 0 \quad C_i(0, t) = C_{i,0} \quad [13a]$$

$$x = L_0 \quad D_k^w \cdot \frac{\partial Ci}{\partial x} = -\eta \cdot \{R_H(C_W, C_H, T) + R_S(C_W, C_S)\} \quad [13b]$$

The partial differential Eq. [9] and [11] have to be solved numerically with the initial conditions of Eq. [12] and the boundary conditions of Eq. [13]. The boundary conditions at the bottom of the feature are based on the assumption that at the end of the feature the diffusive flux towards the bottom is equal to the consumption of the reactant by the chemical reactions.

The partial differential equations were solved numerically using a fully implicit scheme (32). This implicit scheme is stable even for large time steps. The discretization method we used has a first-order accuracy in time and a second-order accuracy in space. For most of the calculations the total trench depth was divided into 20 equidistant pieces. The grid independence was checked for a representative situation using 50 and 100 grid points. The calculated step coverage obtained on these fine grids differed less than 0.5% from those obtained on a standard grid of 20 grid points. The time step was chosen to satisfy the requirement that the concentration change between two time steps did not differ more than 0.1% from the previous calculation. The maximum time step was set to 5 s. We solved the differential equations with full-time dependency. This development differs from (22, 23) where these equations were solved using steady- or pseudo steady-state approximations. McConica *et al.* recently (17) concluded that the steady- or pseudo steady-state solution is only valid for conditions of no significant depletion of the reactants.

In the case of conformal deposition and high aspect ratio features the length of the feature does not change much. In this regard, one should note that for nonconformal feature fillings, the length of the feature is increasing during deposition. In our model we also account for this changing length of the feature during deposition.

Experimental Procedure

The step coverage experiments of tungsten LPCVD were performed in an ASM cold wall single-wafer reactor, which is designed for handling 8 in. wafers. In our experiments an 8 in. wafer is used as carrier for a 3 in. p-type 10 Ω · cm (100) wafer. In all the experiments the deposition area was over the whole 8 in. wafer. A schematic sketch of the reactor and the gas lines is presented in Fig. 6. The walls of the reactor chamber are water cooled. The wafer is placed on a graphite susceptor, which is placed on a quartz dome. The susceptor is heated indirectly by a heating element. Gases are injected radially near the top of the reactor perpendicular into a 0.20 m diam gas tube. This tube is positioned perpendicular to the wafer surface. The purity of the gas sources (WF_6, SiH_4, H_2, Ar) employed for the experiments was 99.999%.

In cold wall LPCVD reactors the temperature of the wafer is not equal to the temperature of the susceptor, but is related to total pressure, gas composition, coating of the wafer, and the temperature of the susceptor. The temperature of the susceptor could be measured by a series of thermocouples. By knowing the temperature of the susceptor, the gas composition, and the total pressure the wafer temperature could be determined from calibration tables with an accuracy of ±5 K. The calibration was done by measuring the temperature of a Si wafer (p^+-0.02 Ω · cm) as a function of the susceptor temperature, the gas composition, and the total pressure. The temperature of the Si wafer (p^+-0.02 Ω · cm) was measured with the use of a dual wavelength pyrometer (2.1 and 2.3 μm).

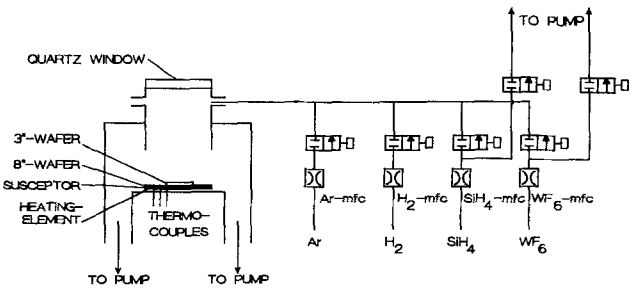

Fig. 6. Schematic sketch of the cold wall reactor and the gas lines.

Trenches and circular holes were reactive ion etched (RIE) using a gas mixture of Cl_2 and $SiCl_4$. The trenches and circular holes were etched with SiO_2 as a mask to a depth of about 10 μm and have a diameter ranging from 1 to 4 μm.

After RIE etching the SiO_2 was removed in HF (1:6). Just before tungsten deposition the wafers received a dip of 30 s in 1% HF. Each tungsten deposition was preceded by an *in situ* deposition of a silicon reduced tungsten film (10 sccm WF_6, 1.5 slm Ar, P_{TOT} = 133 Pa, T_{WAFER} = 673 K) of 25 ± 5 nm (13).

The thickness of the tungsten films and the step coverage was determined by SEM observations. The use of trenches instead of contact holes as a test vehicle for step coverage is very applicable, because cleaves through trenches can be obtained easily and the trench cleaves expose the real deposition profile. Getting straight cleaves through the middle of contact holes of micron dimensions is hardly possible. Cleaves of contact holes that do not go through the middle, reflect a wrong step coverage. This advantage of trenches as a test vehicle for monitoring step coverage has been described earlier by Schmitz *et al.* (1).

The step coverage as calculated by the step coverage model were compared with SEM observations. Absolute step coverages as determined by SEM observations have an overall accuracy of ±5%.

The experiments on step coverage used in this study and the deposition parameters are summed up in Appendix A.

Results

Motivation for using a reactor model.—In order to get precise knowledge of the reactant partial pressures a reactor model is used. The distribution of the reactants are mainly determined by hydrodynamics and transport phenomena. Especially in the case of cold wall single-wafer reactors where deposition rates are high and the walls are cooled, the inlet concentrations do not represent the reactant concentrations just above the wafer surface. These reactant wafer concentrations have to be known in order to calculate the step coverage. The reactor model is used to determine the partial pressures of the reactants just above the wafer surface. These partial pressures are used as input for our step coverage model. In the study (28, 38) of growth rates as function of the inlet flows of WF_6, H_2, and Ar, it became clear that the inlet concentrations in cold wall reactors do not represent the wafer surface concentrations. The conversion rate, which is often used as criterion for gradientless reactor operation, was shown to be not a good criterion, not even in the case of high gas flows. This study also showed the importance of thermal diffusion phenomena. Due to this thermal diffusion, wafer surface partial pressures of WF_6 will always be lower than the inlet partial pressure. Thermal diffusion causes the relatively heavy WF_6 molecules to move away from the hot susceptor. From

Table I. Comparison between different methods to calculate WF_6 partial pressures at the wafer surface.

Exp.	Conversion of WF_6	$p(WF_6)^a$ (Pa)	$p(WF_6)^b$ (Pa)	$p(WF_6)^c$ (Pa)
1	49%	4.66	2.26	1.06
10	13%	3.99	3.59	2.00

[a] $p(WF_6)$ at wafer surface supposed equal to inlet partial pressure.
[b] $p(WF_6)$ at wafer surface supposed equal to outlet partial pressure.
[c] $p(WF_6)$ at wafer surface calculated by reactor model.

the above it is clear that a reactor model which incorporates thermal diffusion effects is necessary for determining the actual reactant concentrations at the wafer surface. Another advantage of the reactor model is the knowledge of reaction by-product partial pressures just above the wafer surface. In that manner, possible influences of by-products on the step coverage can be studied. A detailed description of the reactor model that we used can be found in (28, 33, 38).

As mentioned previously the inlet partial pressure of the reactants, especially WF_6, has to be known for accurately predicting the step coverage. For our step coverage model we used inlet partial pressures which were calculated by the reactor model. Other methods, such as accounting for the conversion of the reactants (outlet partial pressure), as used by others (16, 19, 23) are not accurate, because they do not incorporate thermal diffusion phenomena. In Table I the partial surface pressures of WF_6 have been calculated using three different methods. From Table I, we can conclude that the method of calculation for the WF_6 partial pressure at the wafer surface can result in large differences, even in the case of low conversion, as in experiment 10. The reactor model calculations of the WF_6 partial pressures are much lower than the other calculation methods. The step coverage model using the wafer surface partial pressure as boundary condition for its calculations will also be influenced by the reactant surface partial pressure.

It must be noted that the reactor model predictions of the WF_6 pressure at the wafer surface are relatively sensitive to small errors in the thermal diffusion coefficients, which were obtained from kinetic gas theory. For example, a 25% increase of the thermal diffusion coefficient led to a decrease in the WF_6 surface partial pressure from 1.06 to 0.88 Pa for experiment 1 and from 2.00 to 1.76 Pa for experiment 10. The resulting changes in predicted step coverages for a 2 × 10 μm trench are from 77 to 74% for experiment 1 and from 82 to 80% for experiment 10, respectively.

The hydrogen reduction reaction.—In our step coverage study we did not account for any influence of the by-products on growth rate. For reaction [1] it has been found (29, 34) that HF can supress the tungsten growth rate. Others found that HF did not have more than a dilution effect (35) on deposition rate. It is very difficult to incorporate such influences of by-products in the step coverage modeling because little data are available, and these data are not consistent. In our case using the reactor model we can calculate the partial pressure of HF just above the wafer. If HF had some influence, the growth rate predicted by the reactor model based on Eq. [6] and the experimental results at different HF partial pressures should contradict. Also the step coverages should be influenced by the *in situ* generated HF. Especially inside the trenches or contact holes the by-product partial pressures can be very high during growth.

The influence of HF is examined in four experiments, where the HF partial pressure was varied from 1.2 to 12.3 Pa. These varying partial pressures were achieved by changing total flow while maintaining a constant partial pressure of H_2. The HF and WF_6 partial pressures were calculated by the reactor model. The results of these four experiments are presented in Table II. From these experiments we see that the influence of HF on step coverage is within the experimental error. From this we may conclude

Table II. Influence of HF on step coverage. In all the experiments the partial pressure of H_2 is kept on 110 Pa.

Exp.	$p(WF_6)$ surface (Pa)	$p(HF)$ surface (Pa)	Trench (μm)	Step coverage (%) Exp.	Step coverage (%) Model	Growth rate (nm/min) Exp.	Growth rate (nm/min) Model
1	1.04	12.30	2.0 × 10	73	77	87.2	91.7
2	1.47	5.92	2.6 × 10	80	86	77.4	83.0
3	1.98	2.59	3.2 × 10	92	92	57.4	62.2
4	2.38	1.20	2.4 × 10	89	91	41.8	44.7

that the influence of HF by-product on step coverage is negligible in the examined regime.

In all cases of modeling on the H_2 reduction reaction we found that the primary cause of the drop in step coverage is depletion of WF_6 in the trench. Although the reaction is zero order in WF_6, the reaction rate still becomes zero when the partial pressure of WF_6 becomes zero. This effect of WF_6 depletion is shown in Fig. 7 and 8, where partial pressure profiles of the reactants are shown at several stages during growth, for two typical cases

Figure 7 $-WF_6{:}H_2 = 1{:}1$

Figure 8 $-WF_6{:}H_2 = 1{:}10$

In these two cases the partial pressure of H_2 at the trench inlet was 17 Pa, HF partial pressure was 1.7 Pa, wafer temperature 723 K, resulting in a surface growth rate of about 50 nm/min. The trenches were 2 × 10 μm. From Fig. 7 and 8 we see that the primary cause of the drop in step coverage is WF_6 depletion rather than H_2 depletion, in spite of the three times higher flux of H_2. In general this is because of (*i*) the higher diffusivity of H_2 compared to WF_6 (about 12 times), (*ii*) in almost all cases H_2 is available in excess; and (*iii*) growth rate has only a square root dependence on the H_2 partial pressure. Thus considering the H_2 partial pressure constant [cf. McConica *et al.* (15)] during growth does not influence the predicted value of the step coverage much.

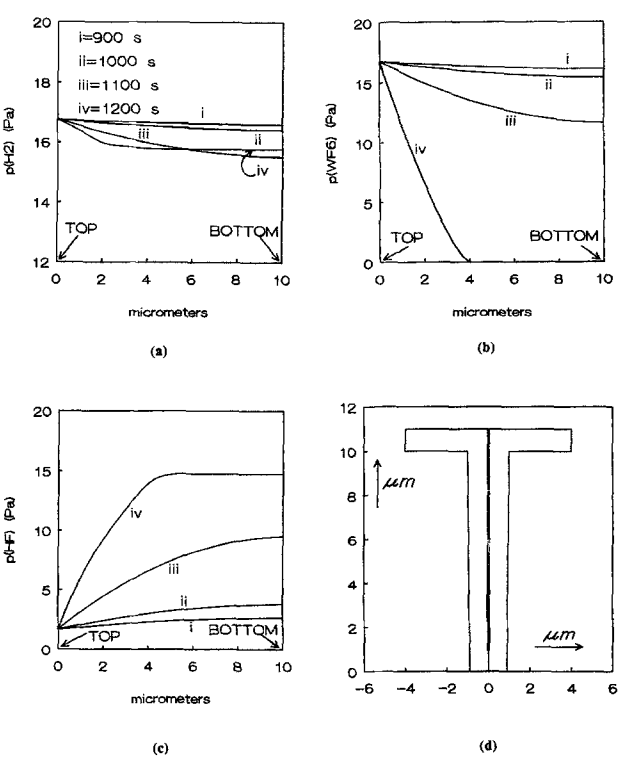

Fig. 7. Time varying partial pressures profiles in 2 × 10 μm trench for $WF_6{:}H_2$ = 1:1 (a-c). Partial pressure at the trench inlet were (a, b) $H_2 = WF_6$ = 17 Pa, (c) HF = 1.7 Pa, T_{wafer} = 723 K, resulting in a bulk growth rate of 50 nm/min. The deposition profile is shown in (d) resulting in a step coverage of 96%.

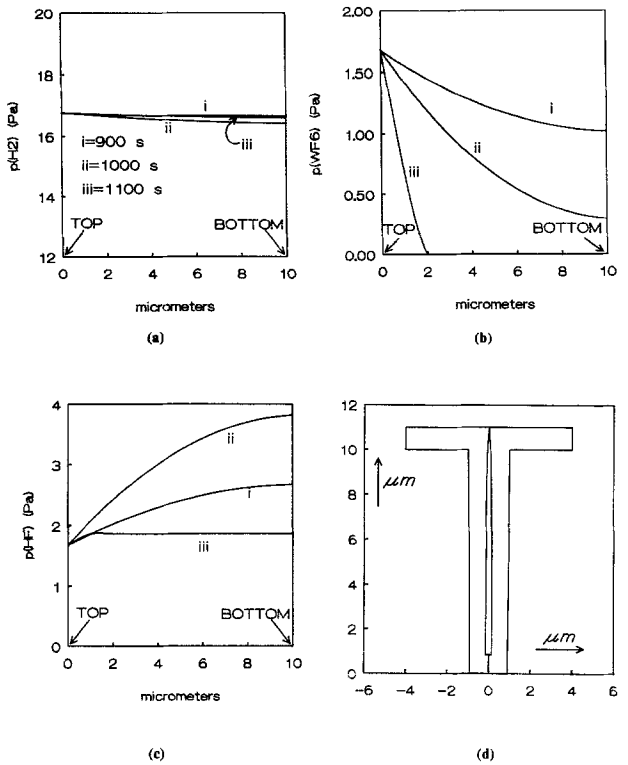

Fig. 8. WF_6:H_2 = 1:10. WF_6 partial pressure at trench inlet is reduced to 1.7 Pa, other parameters as in Fig. 7. In (d) the deposition profile is shown, step coverage drops to 86%.

When the growth rate stops due to a lack of WF_6, we can see a redistribution of the H_2 partial pressure. This effect is shown in Fig. 7a (compare t = 1100 s and t = 1200 s). The partial pressure of HF can be very high deep inside the trench or contact hole, as is shown in Fig. 7c and 8c. The resulting modeled deposition profiles for these two cases are shown in Fig. 7d and 8d.

In Fig. 9 the step coverage of all H_2 reduction reactions is plotted as a function of the so-called step coverage modulus (SCM), first proposed by McConica *et al.* (15). This dimensionless number is given by

$$\mathrm{SCM} = \frac{L_0^2 \cdot R_H}{W_0 \cdot D_k \cdot C_{W,0}} \qquad [14]$$

Figure 9 shows that the model predictions and the experimental values fit well. For simplicity in this figure the changing length during growth is not incorporated, because otherwise a simple S.C. as function of the SCM could not be determined. This makes Fig. 9 only valid for high aspect ratio features. In our experiments, geometries meeting this requirement are used.

The silane reduction reaction.—In the case of the SiH_4 reduction of WF_6 step coverage is not only determined by

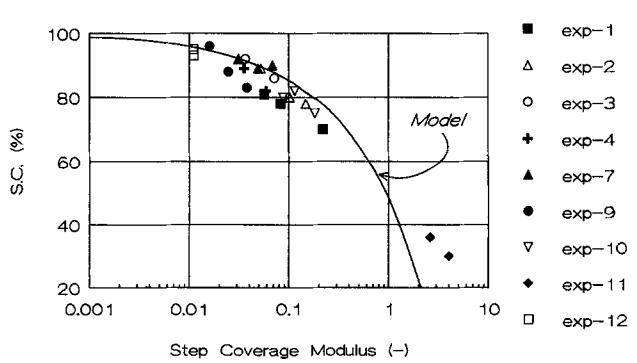

Fig. 9. Step coverage predictions (—) and experiments as a function of the step coverage modulus (SCM).

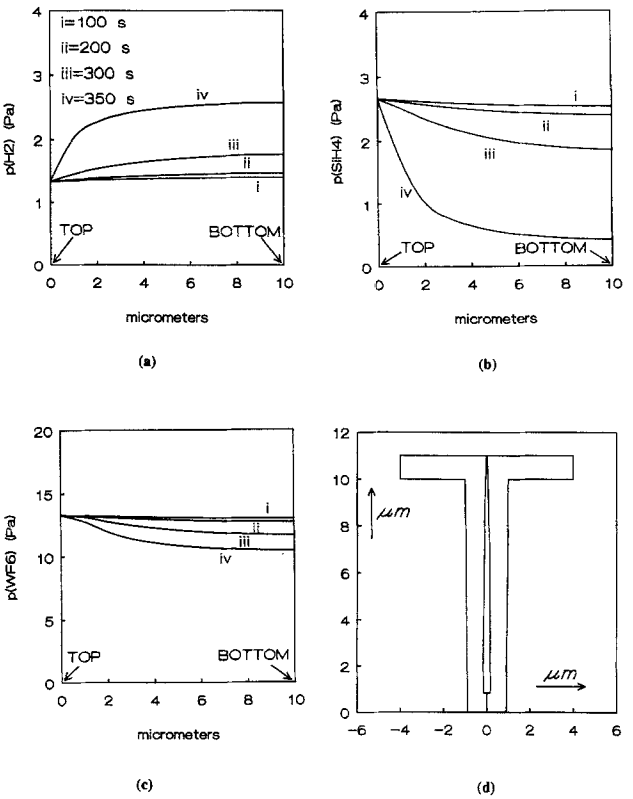

Fig. 10. Time varying partial pressure profiles in a 2 × 10 μm trench. Trench inlet partial pressures were; H_2 = 1.3 Pa, SiH_4 = 2.7 Pa, and WF_6 = 13 Pa. T_{wafer} = 673 K, resulting growth rate 150 nm/min. (a) H_2 partial pressure, (b) SiH_4 partial pressure, (c) WF_6 partial pressure, and (d) deposition profile, resulting S.C. = 84%.

the WF_6 depletion but also by a changing SiH_4 partial pressure in the trench or contact hole. In Fig. 10 and 11 partial pressures and deposition profiles are shown for two cases. First, where step coverage is determined by SiH_4 depletion

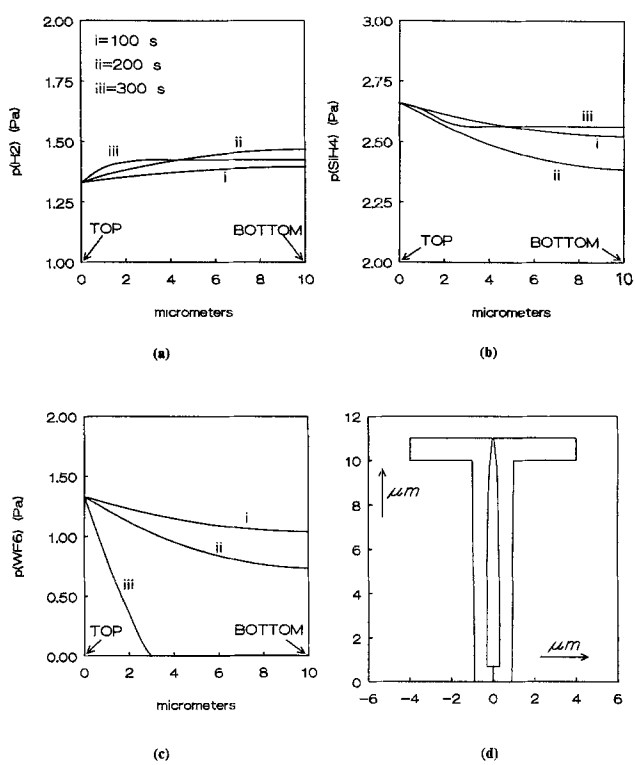

Fig. 11. Parameters as in Fig. 10, except WF_6 partial pressure decreased to 1.3 Pa. (a) H_2 partial pressure, (b) SiH_4 partial pressure, (c) WF_6 partial pressure, and (d) deposition profile, resulting S.C. = 71%.

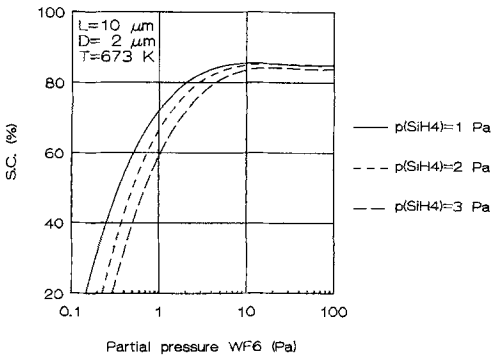

Fig. 12. Step coverage predictions as a function of the partial pressure of WF_6 for three different partial pressures of SiH_4. (a) $p(SiH_4)$ = 1 Pa (—); (b) $p(SiH_4)$ = 2 Pa (----), and (c) $p(SiH_4)$ = 3 Pa (– –).

(see Fig. 10) and, second, step coverage is determined by WF_6 depletion (see Fig. 11). In both modeling cases the growth rate is maintained at about 150 nm/min, temperature is 673 K. At the inlet of the feature the partial pressure of H_2 is kept at 1.3 Pa and the SiH_4 partial pressure is 2.7 Pa. In Fig. 10 WF_6 partial pressure is 13 Pa and in Fig. 11 WF_6 partial pressure is 1.3 Pa. In Fig. 10 the step coverage is determined by SiH_4 depletion and in Fig. 11 by WF_6 depletion. We also see an accumulation of H_2 in the trench, because H_2 is a by-product of the SiH_4 reduction reaction. In the case of SiH_4 reduction reaction, which is first-order in SiH_4, a drop in SiH_4 partial pressure directly results in a lower local growth rate. In that case the step coverage is independent on SiH_4 partial pressure but only dependent on the geometry of the feature. In Fig. 12 the step coverage predictions as a function of the partial pressure of WF_6 at three different partial pressures of SiH_4 are shown. From this figure it can be seen that the model predicts step coverages independent of partial pressure of SiH_4 provided that the partial pressure of WF_6 is sufficiently high. At partial pressures of WF_6 lower than about three times the partial pressure of SiH_4 the step coverage drops. The reason for this is WF_6 depletion rather than SiH_4 depletion. Figure 12 also shows that it is fundamentally impossible to obtain a step coverage of 100% in a 2 × 10 μm trench using the SiH_4 reduction reaction.

The predicted independency of the step coverage on a changing SiH_4 partial pressure at sufficiently high partial pressure of WF_6 is verified experimentally. The results are shown in Table III. From this table we see that the step coverage as predicted by the model is higher than what is seen experimentally. Until now it is not clear why these predicted values of the step coverage are too high. This may be attributed to the fact that very little kinetic data are available for this SiH_4 reduction reaction and the influence of by-products. The influence of SiF_4 on the growth rate, as was shown by Schmitz *et al.* in a single experiment (19), will affect the step coverage to a lower value. Because of the unknown nature and influence of the by-products this is not incorporated in the simulation models.

Experimentally we found no influence of the SiH_4 partial pressure on step coverage at sufficiently high WF_6 partial pressures. This is in agreement with the model predictions and is a clue that the growth rate of the SiH_4 reduction reaction is indeed first order in SiH_4. The step coverage model predicts a drop in step coverage when the WF_6 partial pressure is reduced to a point where step coverage is determined by a lack of WF_6. This is illustrated in two SEM cross sections where the surface partial pressure of SiH_4 is kept constant at about 1.5 Pa but the partial pressure of WF_6 is reduced from 10 to 2.4 Pa. This resulted in a drop of the step coverage from 70 to 50% for the 2 × 10 μm trench, see Fig. 13a and 13b.

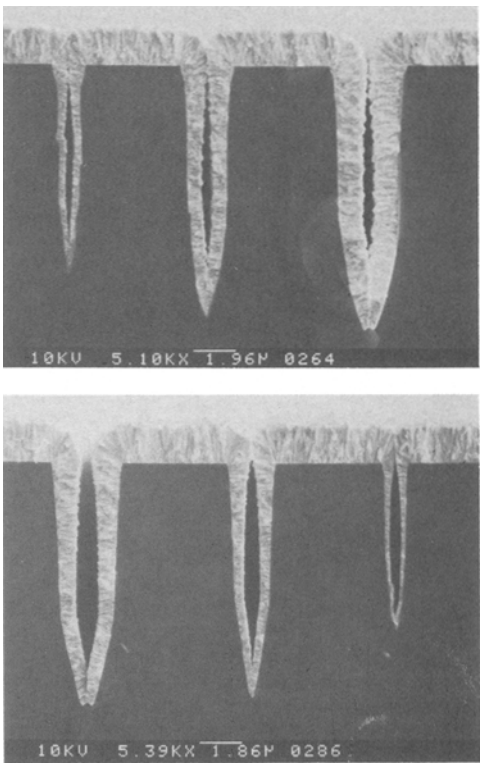

Fig. 13. SEM cross sections for $P(SiH_4)$ = 1.5 Pa, T_{wafer} = 673 K. (a, top) $p(WF_6)$ = 10 Pa and (b, bottom) $p(WF_6)$ = 2.4 Pa. Step coverage in (a) is 70% and in (b) 50% for the 2 × 10 μm trench.

In the case of the SiH_4 reduction reaction of WF_6 the model predicts hardly any influence of the temperature. This is verified in three experiments. The results of these experiments are shown in Fig. 14. Although the predicted values are too high the trend is the same.

Comparison of step coverage in trenches and contact holes.—For obtaining experimental step coverage data, trenches are very convenient, because it is much easier to get cleaves through trenches than through contact holes, especially when they are in the range of a few microns. Another advantage of trenches is that they show the real deposition profile. In Fig. 15 a comparison is made between step coverage values predicted in trenches and contact holes of the same diameter depth ratio. This figure is valid (within a few percent) for the SiH_4 as well as the H_2 reduction reaction.

In one case it was possible to break exactly through a 3.2 × 10 μm contract hole, giving a step coverage of 48%. The trench of 3.2 × 10 μm on the same wafer revealed a step coverage of 76%. This is in very good agreement with Fig. 15 (see dashed line). These cleaves are shown in Fig. 16a and 16b.

Table III. Step coverage in 2.2 × 10 μm trenches at different partial pressures of SiH_4. In these experiments the wafer temperature was 773 K, total pressure 133 Pa. 1.4 slm argon was used as carrier gas.

Exp.	Conversion of WF_6 (%)	$p(WF_6)$ surface (Pa)	$p(SiH_4)$ surface (Pa)	Growth rate (nm/min)	Step coverage experiment (%)	Step coverage model prediction (%)
14	2	10	0.50	30.1	70	84
15	4	10	1.00	56.4	70	84
16	6	10	1.50	87.5	70	84

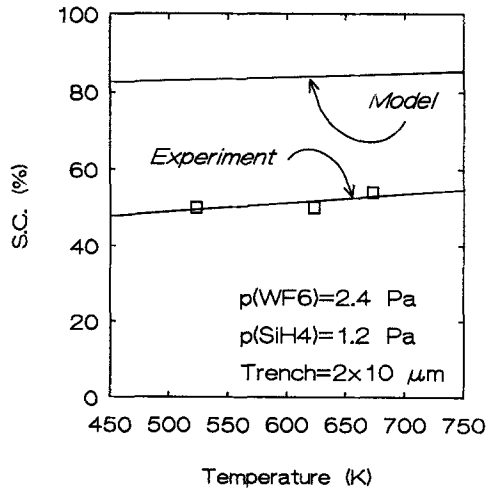

Fig. 14. Influence of temperature on step coverage.

Process optimization.—From the results of the simulations and the experimental verification it is now possible to optimize the step coverage. For this optimization some requirements concerning the W-LPCVD process in a single wafer reactor have been made: (*i*) to get void-free filling of a high aspect ratio contact, step coverage should be 95% in a feature with an aspect ratio of 5, (*ii*) for a throughput of 10 wafers/h, the growth rate should be 150 nm/min, (*iii*) for economic reasons conversion of WF_6 should be high and total WF_6 flow should be low. With the use of the reactor model and the step coverage model these demands could be fulfilled. If a step coverage of 95% is required in a feature with aspect ratio of 5 the SiH_4 reduction reaction, as we saw before (see Fig. 12), is not suitable. So we have to choose the H_2 reduction reaction.

From Eq. [6] we see that we have to increase the partial pressure of H_2 and temperature to obtain a high growth rate. With regard to multilevel metallization the maximum temperature is limited to 693 K, but if we increase the growth rate by increasing the $p(H_2)$, step coverage drops, see Eq. [14]. However, another way to increase $p(H_2)$ is to increase total pressure [$P_{TOT} = p(H_2) + p(WF_6) + p(Ar)$]. In that case the $\sqrt{p(H_2)}/p(WF_6)$ ratio decreases and so does the step coverage modulus (36), see Eq. [14]. In that way the step coverage improves. With a little adaptation of our reactor it was possible to increase the total pressure to 1330 Pa. In that pressure range diffusion in the trenches and contact holes is still dominated by Knudsen diffusion.

For economic use of WF_6, its conversion should be high and the WF_6 flow should be low. To fulfill this demand we calculated the partial pressure of WF_6 at the wafer surface as function of the WF_6 inlet flow at low total flow (see Fig. 17). For a step coverage of at least 95% in a 2 × 10 μm trench and a growth rate of 150 nm/min the step coverage model calculates that the partial pressure of WF_6 should be greater than 30 Pa, so the WF_6 inlet flow has to be greater than 40 sccm. To be on the safe side a WF_6 inlet flow of 50 sccm is chosen. The result of this experiment can be seen in the SEM cross section in Fig. 18.

During deposition the aspect ratio of a trench or a contact hole is changing from the initial diameter length ratio to infinite. So at the start of the deposition the WF_6 partial pressure can be chosen at a lower level than at the end of deposition when the feature is closing. In Fig. 19 we calculated the required WF_6 partial pressure at the wafer surface as a function of the deposition time in such a manner that we maintained a WF_6 partial pressure greater than zero at the bottom of a 2 × 10 μm trench. From this figure we see that in the beginning the WF_6 partial pressure can be lower to ensure a final step coverage of 95%. In Fig. 19 it is also

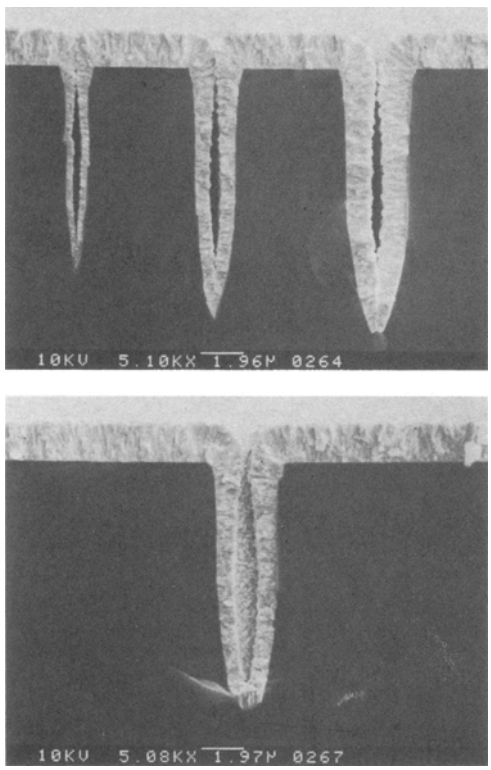

Fig. 16. Cleaves through (a, top) trenches and (b, bottom) a contact hole.

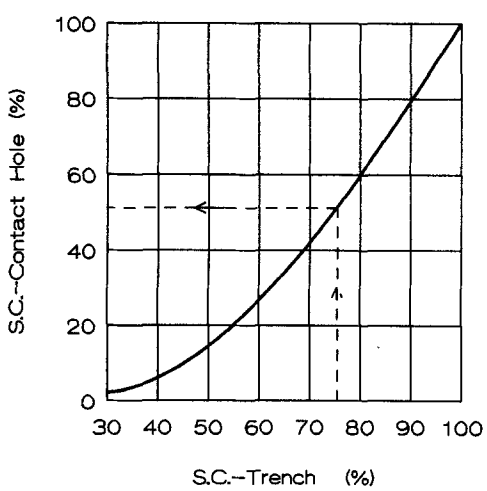

Fig. 15. Comparison of S.C. in trenches and contact holes.

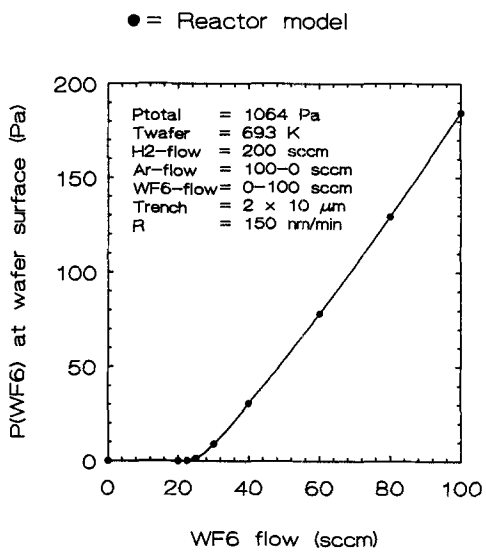

Fig. 17. Partial pressure of WF_6 at the wafer surface as a function of the WF_6 inlet flow.

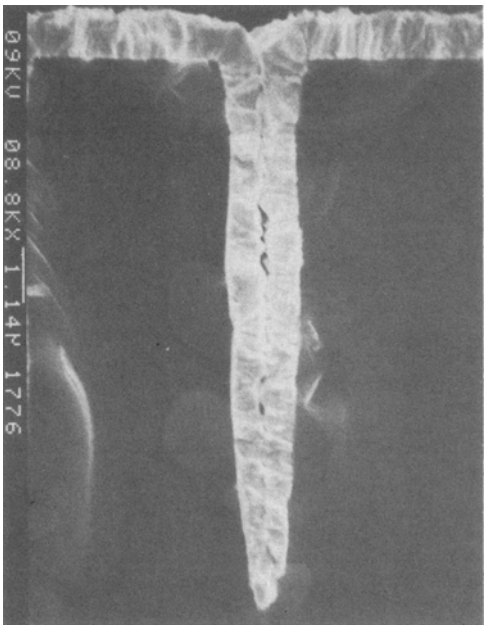

Fig. 18. Cross section of a trench, P_{total} = 1064 Pa, T_{wafer} = 693 K, H_2 = 200 sccm, Ar = 50 sccm, and WF_6 = 50 sccm. Growth rate is 150 nm/min.

indicated what the WF_6 inlet flow was in the experiment (see dashed line). The result of this experiment with a changing WF_6 inlet flow and constant total flow during deposition is shown in the SEM picture of Fig. 20. Here we see that the step coverage of this process is equal to the step coverage found by maintaining a constant WF_6 inlet flow of 50 sccm; compare Fig. 18 with 20. As calculated by the reactor model for these two experiments the partial pressure of HF becomes extremely high, about 300 Pa. Note that in spite of this extreme high HF partial pressure we found no influence on step coverage and growth rate. Step coverage as well as growth rate are in agreement with the step coverage and reactor model, respectively.

With this process using the more economic WF_6 inlet flow and high total pressure, contact holes of 2 μm in diameter and 0.8 μm in depth were filled. After RIE back etching in a chlorine containing plasma no void could be detected, see SEM picture in Fig. 21. A conformal step coverage is obtained, otherwise a top view should reveal a hole in the middle of the contact. In Fig. 21 some attack of the RIE plasma on the oxide can be observed.

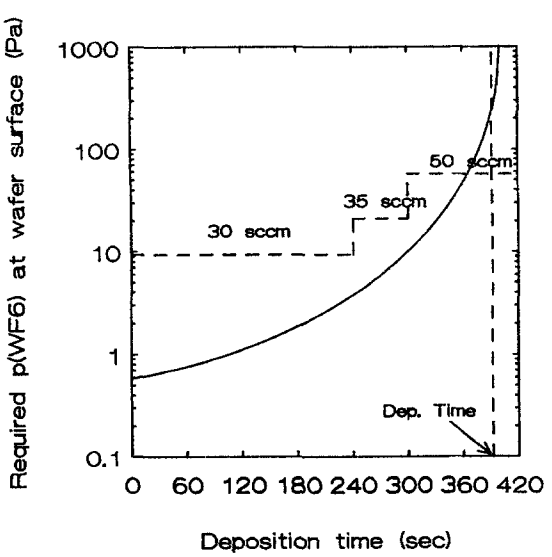

Fig. 19. Required partial pressure at wafer surface enough to maintain growth on the bottom of a 2 × 10 μm trench as a function of the deposition time. Calculated (—) and experimental (----).

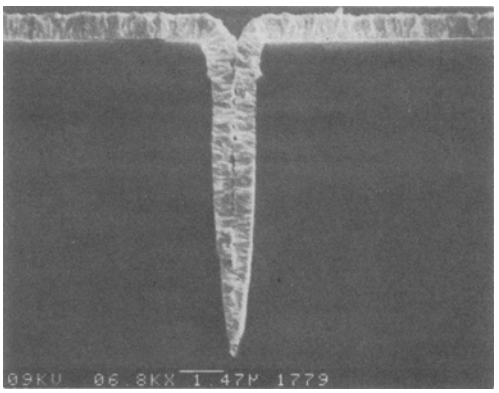

Fig. 20. Cross section of a trench, P_{total} = 1064 Pa, T_{wafer} = 693 K, H_2 = 200 sccm, Ar varying from 70 to 50 sccm, and WF_6 varying from 30 to 50 sccm. Growth rate is 150 nm/min.

Discussion

Until now it is not clear why the predicted values of the step coverage in the case of the SiH_4 reduction reaction are too high. This may be due to a lack in the knowledge of the true kinetics of the SiH_4 reduction reaction and the unknown influence of by-products. However, the trends predicted by the step coverage model were in good agreement with the experiments. From the modeling studies and the experimental observations it is very likely that the SiH_4 reduction reaction of WF_6 is indeed first order in SiH_4.

From a fundamental point of view the SiH_4 reduction reaction offers no advantages in terms of step coverage over the H_2 reduction reaction. First, the step coverage is worse than the H_2 reduction reaction and the step coverage cannot be tuned to a value near 100% for (sub)micron contact holes. This is because the SiH_4 reduction reaction is first order in SiH_4. For first-order reactions, step coverage is independent of the partial pressure of the reactant. A second reason for the lower step coverage for the SiH_4 reduction reaction is the higher rate constant than the H_2 reduction reaction at comparable partial pressures. Another problem with the SiH_4 reduction reaction is that the SiH_4/WF_6 ratio is extremely important for contact resistance and grain structure (8, 9, 11, 37). Because of the difference of Knudsen diffusivity between WF_6 and SiH_4 during deposition a change of the ratio of these two reactants can occur easily down to the length of a trench or contact hole. The tungsten of the bottom could contain tungsten silicide which has a much higher resistance. This problem can be avoided by working in an excess of WF_6.

For the H_2 reduction reaction a good fit of experimental step coverage data and step coverage modeling was found provided we use the reactor model in order to calculate the

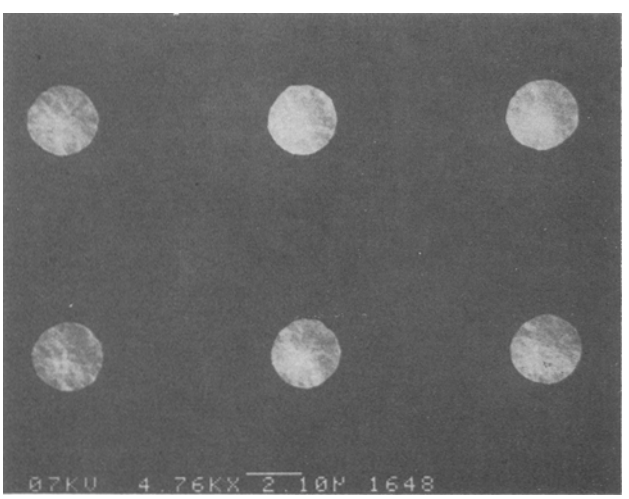

Fig. 21. Contact holes (2 × 0.8 μm) filled with a varying WF_6 partial pressure and etched back in a chlorinated plasma.

surface reactant partial pressures. The reactor model showed that keeping reactive areas small and flow rates high is not enough to ensure that the inlet concentrations do represent the wafer surface concentrations. This in contrast to the suggestion of Chatterjee *et al.* (23). Thermodiffusion strongly affects the reactant concentration profiles in cold wall reactors, especially in the case of a mixture of WF_6 and H_2 (28, 38).

Conclusions

In the case of the H_2 reduction reaction a good agreement between the experimental step coverage data and model is found. The step coverage is determined by the depletion of WF_6 in the feature. No influence of HF is found on step coverage. The step coverage in high aspect ratio features is enhanced by high WF_6 partial pressure and low growth rate.

A reactor model is needed to predict true surface concentrations. True concentrations cannot be calculated just by calculating conversion because thermodiffusion plays an important role in the distribution of a gas mixture, especially in the case of a gas mixture containing WF_6 and H_2. Although high throughput and high step coverage are contradictory goals, we were able to define a process which combines both. Using the step coverage and reactor model a process is obtained with high step coverage, high conversion of WF_6, low flow of WF_6, and high growth rate.

Process characterization:

P_{TOTAL}	=	1064 Pa
T_{WAFER}	=	693 K
H_2 flow	=	200 sccm
WF_6 flow	=	30-50 sccm (varying)
Ar flow	=	70-50 sccm (varying)
Growth rate	=	150 nm/min
Step coverage	≥	95% in feature with aspect ratio of 5 and uniform over a 6 in. wafer

The step coverage of the SiH_4 reduction reaction were proven to be independent of the partial pressure of SiH_4 at sufficiently high partial pressure of WF_6. In that case, the step coverage is only dependent on the aspect ratio of the feature. These experimentally found trends were in agreement with the model predictions, although the absolute predicted values were too high. This may be attributed to a lack in knowledge of the exact kinetics of the SiH_4 reduction reaction and the unknown influences of by-products.

Apart from high growth rate and low surface roughness the SiH_4 reduction reaction offers no fundamental advantages over the H_2 reduction reaction in terms of getting high step coverage.

The step coverage differences as found in trenches and contact holes agree with calculations. Although trends in step coverage found in trenches and contact holes are the same, the absolute values are not.

Acknowledgment

This work forms part of the "Innovatief Onderzoeks Programma IC Technologies" (Innovating Research Program for IC Technology) and was made possible by the financial support from the Netherlands Ministry of Economic Affairs. Bert Otter is also acknowledged for his SEM assistance.

Manuscript submitted Aug. 24, 1990; revised manuscript received Dec. 18, 1990.

The University of Twente assisted in meeting the publication costs of this article.

LIST OF SYMBOLS

A	feature cross-section area, cm^2
A_A	active surface area for deposition, cm^2
C	concentration of any component, $mol \cdot cm^{-3}$
C_i	concentration of component i, $mol \cdot cm^{-3}$
$C_{i,0}$	concentration of component i at inlet feature, $mol \cdot cm^{-3}$
c_1	hydrogen reduction reaction rate constant, $mol \cdot Pa^{-1/2} \cdot cm^{-2} \cdot s^{-1}$
c_2	silane reduction reaction rate constant, $mol \cdot Pa^{-1} \cdot cm^{-2} \cdot s^{-1}$
D_k	Knudsen diffusivity of any component, $cm^2 \cdot s^{-1}$
$D_{k,\infty}$	Knudsen diffusivity in infinite geometries, $cm^2 \cdot s^{-1}$
D_k^i	Knudsen diffusivity of component i, $cm^2 \cdot s^{-1}$
E_A	activation energy, $kJ \cdot mol^{-1}$
K′	Clausing's factor
L_0	initial feature depth, cm
l	variable feature depth, cm
M	mole weight, $g \cdot mol^{-1}$
p(i)	partial pressure of component i, Pa
R	gas constant, $kJ \cdot mol^{-1} \cdot K^{-1}$
R_0	initial radius of contact hole, cm
r	variable radius of contact hole, cm
R_H	deposition rate due to hydrogen reduction reaction, $mol \cdot cm^{-2} \cdot s^{-1}$
R_S	deposition rate due to silane reduction reaction, $mol \cdot cm^{-2} \cdot s^{-1}$
S.C.	step coverage based on film thickness at half-feature depth, %
SCM	step coverage modulus
T	absolute temperature, K
t	time, s
V	volume, cm^3
W_0	initial width of trench, cm
w	variable width of trench, cm

APPENDIX A

Experiments on step coverage

Exp. (—)	WF_6 (sccm)	H_2 (sccm)	Ar (sccm)	SiH_4 (sccm)	P_{TOT} (Pa)	T_{wafer} (K)	Growth rate Exp. (nm/min.)	Growth rate Model (nm/min.)
1	20	500	46	0	133	703	87.2	91.7
2	35	1000	131	0	133	698	77.4	83.0
3	65	2000	300	0	133	678	57.4	62.2
4	125	4000	639	0	133	663	41.8	44.7
7	26	432	425	0	133	683	62.7	70.3
8	18	132	435	0	133	683	35.2	39.8
9	13	371	49	0	133	648	33.3	36.6
10	85	2400	315	0	133	713	98.5	105.4
11	5	2400	395	0	133	673	41.1	24.1
12	50	200	50	0	1064	693	143	150.0
13	30-50	200	70-50	0	1064	693	135	150.0
13b	With back etching on diodes (see SEM picture Fig. 21)						—	—
14	150	0	1331	70	133	673	140	144.9
15	150	0	1371	42	133	673	87.5	86.7
16	150	0	1391	28	133	673	56.4	57.8
17	150	0	1411	14	133	673	30.1	28.8
18	25	0	500	20	133	673	69.0	110.0
19	25	0	500	20	133	523	69.0	110.0
20	25	0	500	20	133	623	69.0	110.4

x distance along feature length, cm

Greek

η stoichiometry constant
ρ_w solid density of deposited tungsten, mol · cm^{-3}

Subscripts

w tungstenhexafluoride, WF_6
s silane, SiH_4
H hydrogen, H_2
HF hydrogen-fluoride, HF
SiF_4 silicon-tetra-fluoride, SiF_4
0 at inlet of feature

Superscripts

w tungstenhexafluoride, WF_6
s silane, SiH_4
H hydrogen, H_2
HF hydrogen-fluoride, HF
SiF_4 silicon-tetrafluoride, SiF_4

REFERENCES

1. J. E. J. Schmitz, R. C. Elwanger, and A. J. M. Dijk, in "Tungsten and Other Refractory Metals for VLSI Applications III," V. A. Wells, Editor p. 55, MRS Pub., Pittsburgh (1988).
2. R. Blumenthal and G. C. Smith, *ibid.*, p. 47.
3. E. K. Broadbent and C. L. Ramiller, *This Journal*, **131,** 1427 (1984).
4. E. K. Broadbent and W. T. Stacy, *Solid State Technol.*, **28,** 51 (1985).
5. C. M. McConica and K. Krishnamani, *This Journal*, **133,** 2542 (1986).
6. Y. Kushumoto, K. Takakuwa, H. Hashinokuchi, and I. Nakayama, in "Tungsten and Other Refractory Metals for VLSI Applications III," V. A. Wells, Editor, p. 103, MRS Pub., Pittsburgh (1988).
7. R. F. Foster, S. Tseng, L. Lane, and K. Y. Ahn, in *ibid.*, p. 69.
8. T. Ohba, T. Suzuki, T. Hara, Y. Furumura, and K. Wada, in "Tungsten and Other Refractory Metals for VLSI Applications IV," R. S. Blewer, and C. M. McConica, Editors, p. 17, MRS Pub., Pittsburgh (1989).
9. J. E. J. Schmitz, M. J. Buiting, and R. C. Elwanger, *ibid.*, p. 27.
10. K. Y. Ahn, P. M. Fryer, J. M. E. Harper, R. V. Joshi, C. W. Miller, and E. G. Colgan, *ibid.*, p. 35.
11. R. S. Rosler, J. Mendoca, and M. J. Rice, *J. Vac. Technol. B*, **6,** 1721 (1988).
12. R. J. Saia, B. Gorowitz, D. Woodruff, and D. M. Brown, *This Journal*, **135,** 936 (1988).
13. J. Holleman, A. Hasper, and J. Middelhoek, in "Chemical Vapor Deposition of Refractory Metals and Ceramics," T. M. Besman, and B. M. Gallois, Editors, p. 107, MRS Pub., Pittsburgh (1989).
14. J. E. J. Schmitz, A. J. M. van Dijk, and M. W. M. Graef, in "Tenth International Conference on Chemical Vapor Deposition," G. W. Cullen, Editor, PV 87-7, p. 625, The Electrochemical Society Softbound Proceedings Series, Pennington, NJ (1988).
15. C. M. McConica and S. Churchill, in "Tungsten and Other Refractory Metals for VLSI Applications III," V. A. Wells, Editor, p. 257, MRS Pub., Pittsburgh (1988).
16. C. M. McConica, S. Chatterjee, and S. Sivaram, Paper presented at Fifth Annual IEEE VLSI Multilevel Interconnection Conference, Santa Clara, CA, 1988.
17. C. M. McConica and A. S. Inamdar, in "Tungsten and Other Refractory Metals for VLSI Applications IV," R. S. Blewer and C. M. McConica, Editors, p. 197, MRS Pub., Pittsburgh (1989).
18. T. S. Cale, F. A. Shemansky, G. B. Raupp, *ibid.*, p. 183.
19. J. E. J. Schmitz, W. L. N. van der Sluys, and A. H. Montree, in "Tungsten and Other Advanced Metals for VLSI/ULSI Applications V," S. S. Wong and S. Furukawa, Editors, p. 117, MRS Pub., Pittsburgh (1990).
20. A. Hasper, C. R. Kleijn, J. Holleman, and J. Middelhoek, *ibid.*, p. 127.
21. E. J. McInerney, P. Geraghty, and S. Kang, *ibid.*, p. 135.
22. G. B. Raupp and T. S. Cale, *Chem. Mater.*, **1,** 207 (1989).
23. S. Chatterjee and C. M. McConica, *This Journal*, **137,** 328 (1990).
24. I. A. Blech, D. B. Fraser and S. E. Haszko, *J. Vac. Sci. Technol.*, **15,** 13 (1978); Errata, *J. Vac. Sci. Technol.*, **15,** 1856 (1978).
25. M. Knudsen, "The Kinetic Theory of Gases," John Wiley & Sons, Inc., New York (1950).
26. S. Dushman in "Scientific Foundations of Vacuum Technique," J. M. Lafferty, Editor, John Wiley & Sons, Inc., New York (1962).
27. P. Clausing, *Physica*, **9,** 65 (1929).
28. C. R. Kleijn, A. Hasper, J. Holleman, C. J. Hoogendoorn, and J. Middelhoek, in "Tungsten and Other Advanced Metals for VLSI/ULSI Applications V," S. S. Wong and and S. Furukawa, Editors, p. 109, MRS Pub., Pittsburgh (1990).
29. Y. Pauleau and Ph. Lami, *This Journal*, **132,** 2779 (1985).
30. W. A. Bryant, *ibid.*, **125,** 1534 (1978).
31. M. L. Yu, B. N. Eldridge, and R. V. Joshi in "Tungsten and Other Refractory Metals for VLSI Applications IV," R. S. Blewer and C. M. McConica, Editors, p. 221, MRS Pub., Pittsburgh (1989).
32. W. H. Press, S. A. Flannery, S. A. Teukolski, and W. T. Vetterling, "Numerical Recipes in C," Cambridge University Press (1988).
33. C. R. Kleijn, Th. H. van der Meer, and C. J. Hoogendoorn, *This Journal*, **136,** 3423 (1989).
34. J. F. Berkeley, A. Brenner, and W. E. Reid, *ibid.*, **114,** 561 (1976).
35. H. Cheung, in "Proceedings of the 3rd International Conference on Chemical Vapor Deposition," F. A. Glaski, Editor, p. 136, The American Nuclear Society, Hinsdale, IL (1970).
36. J. E. J. Schmitz, A. J. M. van Dijk, J. L. G. Suijker, M. J. Buiting, and R. C. Elwanger, in "Proceedings of the European Workshop on Refractory Metals and Silicides," R. De Keersmaekers and K. Maex, p. 350, North-Holland, Pub. Co., Amsterdam (1989).
37. C. A. van der Jeugd, A. H. Verbruggen, G. J. Leusink, G. C. A. M. Janssen, and S. Radelaar, in "Tungsten and Other Advanced Metals for VLSI/ULSI Applications V," S. S. Wong and S. Furukawa, Editors, p. 267, MRS Pub. Pittsburgh (1990).
38. C. R. Kleijn, A. Hasper, J. Holleman, C. J. Hoogendoorn, and J. Middelhoek, *This Journal*, **138,** 509 (1991).